(d,n) proton-transfer reactions on ^{9}Be, ^{11}B, ^{13}C, ^{14,15}N, and ^{19}F and spectroscopic factors at $E_d = 16$ MeV

M. Febbraro,* F. D. Becchetti, R. O. Torres-Isea, J. Riggins, and C. C. Lawrence†
Physics Department, University of Michigan, Ann Arbor, Michigan 48109, USA

J. J. Kolata and A. M. Howard‡
Physics Department, University of Notre Dame, Notre Dame, Indiana 46556, USA
(Received 9 February 2017; revised manuscript received 12 July 2017; published 18 August 2017)

The (d,n) reaction has been studied with targets of ^{9}Be, ^{11}B, ^{13}C, ^{14,15}N, and ^{19}F at $E_d = 16$ MeV using a deuterated liquid-scintillator array. Advanced spectral unfolding techniques with accurately measured scintillator response functions were employed to extract neutron energy spectra without the need for long-path neutron time-of-flight. An analysis of the proton-transfer data at forward angles to the ground states of the final nuclei, using finite-range distorted-wave Born approximation analysis with common bound-state, global, and local optical-model parameter sets, yields a set of self-consistent spectroscopic factors. These are compared with the results of several previous time-of-flight measurements, most done many years ago for individual nuclei at lower energy and often analyzed using zero-range transfer codes. In contrast to some of the earlier published data, our data generally compare well with simple shell-model predictions, with little evidence for uniform quenching (reduction from shell-model values) that has previously been reported from analysis of nucleon knock-out reactions. Data for low-lying excited states in ^{14}N from ^{13}C(d,n) also is analyzed and spectroscopic information relevant to nuclear astrophysics obtained. A preliminary study of the radioactive ion beam induced reaction ^{7}Be(d,n), $E(^{7}\mathrm{Be}) = 30$ MeV was carried out and indicates further improvements are needed for such measurements, which require detection of neutrons with $E_n < 2$ MeV.

DOI: 10.1103/PhysRevC.96.024613

I. INTRODUCTION

There are many nuclear spectroscopic measurements involving detection of an outgoing light charged particle, and in particular, (d,p), (d,t), $(^{3}\mathrm{He},d)$, etc. However, there are far fewer measurements involving detection of an outgoing neutron, as for example the (d,n) reaction, the analog to the (d,p) reaction, and the (α,n) reaction. Several of the latter are important as spectroscopic tools and also can provide information on the corresponding radiative capture reactions (n,γ), (p,γ), and (α,γ), respectively, which are important in astrophysics [1–4]. The problem of course is that energetic neutrons often must be detected via a recoil proton in an organic scintillator using long-path time-of-flight to obtain the outgoing neutron energy spectrum. Such a measurement usually has low overall efficiency since the incident beam must be narrowly bunched (e.g., a few ns wide) and then pulse selected (typically one in four or more) to obtain an appropriate neutron time-of-flight (ToF) spectrum. Likewise the angular range covered by the ToF detector array, often a large "wall" of scintillators, may be limited. The situation is especially unfavorable when a low-intensity secondary radioactive ion beam (RIB) is utilized or low cross section sub-barrier measurements are needed ([1,5], and Sec. V).

Fortunately as noted by Brooks and co-workers [6,7], *deuterated* scintillators can exploit the fact that the $n+d$ cross sections, unlike $n+p$ cross sections, are asymmetric for neutron energies in the range of a few keV to >50 MeV. This results in a forward-going recoil deuteron in the scintillator, produced with most of the incident neutron energy [i.e., $E_{d,\,\mathrm{max}} = (8/9)E_n$]. Thus, a distinct peak in the scintillator light spectrum is generated with a peak location directly related to the incident neutron energy [7–16]. However, the extraction of high-quality neutron energy spectra was limited in the past by the lack of accurate detector response data and the computing power needed to unfold the detector spectra. In recent years, the use of waveform digitizers for digital signal processing (DSP) now permits much-improved neutron detector systems based on deuterated scintillators, including organic liquid and crystal scintillators. In particular, neutron-γ digital pulse-shape discrimination (PSD) has made it possible to develop improved algorithms for optimal particle identification in liquid scintillators. Also, many of the detector response functions needed for accurate spectral unfolding using DSP to produce good neutron energy spectra from deuterated scintillators are now available [14–19].

In this work we exploit the above improvements in deuterated scintillators and DSP to make a set of (d,n) nuclear reaction measurements for several nuclei, $A < 20$. In Sec. II we describe the techniques used to extract neutron spectra from unfolding of the light spectra. In Secs. III and IV we present the ground state (g.s.) cross sections and discuss the systematics of g.s. spectroscopic factors in these

*Present address: Physics Division, Oak Ridge National Laboratory, Oak Ridge, TN 37381; febbraromt@ornl.gov
†Present address: Kennedy School of Government, Harvard University, Cambridge, MA 02138.
‡Present address: Technische Universität München, D-85748 Garching, Germany.

nuclei, deduced in a self-consistent manner using finite-range distorted-wave Born approximation (FR-DWBA). In addition, we present an analysis of low-lying states in ^{14}N observed in ^{13}C(d,n) and spectroscopic information obtained relevant to nuclear astrophysics. Comparisons with earlier, selected cross section measurements using traditional long-path n-ToF are also discussed. The latter were performed by several different groups many years ago (>40 years for data cited here), and much of the spectroscopic information published, mostly obtained using zero-range DWBA (ZR-DWBA), often is not in agreement between different measurements. Also, unlike the present measurements, several of the older experiments used partially enriched isotopic targets and thus often had background peaks in the neutron spectra from other isotopes in the target (see Sec. IV). Finally, in Sec. V we present a preliminary measurement of the ^{7}Be(d,n) reaction using the deuterated scintillator array and note improvements needed for this type of radioactive-beam experiment.

II. (d,n) MEASUREMENTS

The detectors used here have permitted a systematic study of the (d,n) reaction on several nuclei, $A < 20$, well above the Coulomb barrier, i.e., at higher bombarding energy than many of the earlier measurements, in a single set of experiments. The results could then be analyzed with FR-DWBA in a self-consistent manner to extract spectroscopic information for these nuclei. Given the relatively new detector system and related techniques being used to extract neutron energy spectra and cross sections, we describe some of the important experimental details.

Solid targets of deuterated polyethylene $[C_2D_4]_n$ [where "D" denotes deuterium (^{2}H)], ^{9}Be, ^{11}B, ^{13}C and gaseous targets of $^{nat}N_2$, $^{15}N_2$, and ^{19}F as SF_6 were used. Several (d,n) cross sections for these targets and most level schemes of the populated final nuclei are known and thus provide an ideal reference set for the measurements. However as noted, much of the existing data were taken many years ago, often at lower energies where direct reactions may not dominate, at times were limited in the angular range covered, and the spectroscopic information obtained by various authors on a given nucleus often is in disagreement.

A. Experimental setup

The (d,n) measurement campaign was conducted at the University of Notre Dame's (ND) Nuclear Science Laboratory (NSL). The deuteron beam was produced by the NSL FN tandem Van de Graaff accelerator at $E_d = 16.0$ MeV. The beam current on the target was typically limited to 0.2–10.0 electrical nanoamps (enA) to minimize pulse pile up. A 1.9 cm thick, electrically isolated graphite beam stop, which served as a Faraday cup for accurate beam-charge integration, was fabricated as part of a low-background beam dump. The Faraday cup and beam dump were encased in a 60 cm × 60 cm × 60 cm paraffin-lined lead cave to reduce beam-induced background. Borated polyethylene pellets and plastic boron-loaded water jugs were used for additional shielding. A 25 cm diameter thin-wall (approximately 3 mm) stainless-steel scattering chamber was equipped with a movable detector mount which permitted rotation of a silicon ΔE-E telescope detector in vacuum to known scattering angles. In addition to the Faraday cup, the beam flux through the target was monitored using elastic scattering of the deuteron beam into a silicon detector telescope that was kept at a fixed forward angle. Both 4 in. diameter × 6 in. deep (4 × 6) and 2 in. diameter × 2 in. deep (2 × 2) EJ315 detectors were used in these measurements. The 4 × 6 detectors are shown surrounding the target chamber in Fig. 1. The entrance windows of the 4 × 6 detectors were located at a radius of 1.0 m and those of the 2 × 2 detectors at 50 cm with respect to the central target position. The detectors thus subtended approximately the same angular acceptances and solid angles. However, values for the latter were accurately calculated taking into account the finite size of the detectors. This permitted short-path n-ToF with a moderately bunched beam but without need for a pulse-selected beam (hence not much loss in beam intensity). This gave suppression of the prompt γ flash in addition to n/γ PSD and also allowed the use of a shadow bar to deduce the presence of room-return neutrons. Unlike many long-path n-ToF measurements, the latter proved to be negligible owing to the high collection efficiency of the EJ315 array.

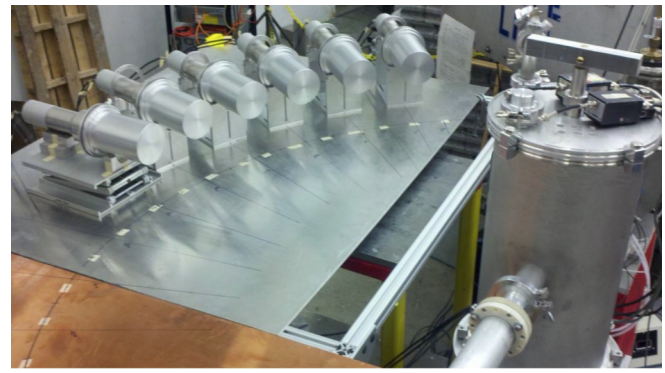

FIG. 1. The experimental setup used in the (d,n) measurements. The array of 4 × 6 EJ315 detectors is shown positioned with the detector entrance windows 1 m from the target.

The detector PMT outputs were digitized with a CAEN V1751 10 bit, 1 GS/s VME module located near the array. The PMT gains were set high (but still linear) to improve the signal-to-noise (S/N) in the anode signals. The signals were then attenuated at the digitizer using high-quality GHz attenuators to match the limited input voltage range of the digitizer. Optimizing the S/N in the scintillator signals and associated cabling is important to provide good pulse-shape analysis of the signals for n/γ discrimination. It also is needed for accurate unfolding of the neutron light spectrum to provide a good neutron energy spectrum. The digitized signals were then sent to a remote data acquisition computer, where a pair of terabyte disks were used to event-store the digitized pulses for post analysis [14,16]. The online data were sampled and displayed during the run to verify that the system was operating correctly. One or more detectors were overlapped between runs to provide accurate angular distributions, including data to far back angles.

B. Preparation of the solid and gaseous targets

Deuterated polyethylene foils $[C_2D_4]_n$ were prepared by an evaporation method using a $[C_2D_4]_n$ powder + xylene solution [16]. A relatively uniform 1.4 mg/cm^2 foil was then selected for use as a target. The ^{9}Be, ^{11}B, ^{nat}C, ^{13}C targets were thin foils ranging from 0.4 to 6.0 mg/cm^2 in thickness, with isotopically enriched (>95%) material used for the ^{13}C target. Most of the solid targets were self-supporting foils except for one of the two ^{13}C targets used, which was on a thin Mylar backing. The other was a commercial ^{13}C foil (Arizona Carbon Foil Co, Tucson, AZ). Owing to the large positive ^{13}C(d,n) Q value, interference from the backing elements (^{12}C in particular) was not an issue as we are mainly using the distinct, high-energy recoil-deuteron peaks for cross-section measurements.

A thin-window cell for the gaseous targets was fabricated with 3 mm thick side walls from free-cutting brass (Alloy 360). The latter was chosen for its low Q values for (d,n) reactions within the alloy and for its high machinability. The low (d,n) Q values result in (d,n) reaction neutrons from the gas cell produced with energies lower than those detected in the reactions of interest, which have more positive (d,n) Q values. The gas cell has 1.0 cm diameter hermetically sealed entrance and exit windows that can be easily changed in case of failure. A 10 μm Havar® metal foil was used as the window material. The gas handling system was located outside of the vacuum chamber through a vacuum feedthrough which allowed for easy and fast gas changes during experimental runs. Digital temperature and absolute pressure gauges monitored gas parameters throughout a run for an accurate target thickness determination.

C. Detector efficiency (peak and total)

In most measurements involving the detection of neutrons the largest source of uncertainty typically is the neutron detection efficiency which usually is light-output threshold dependent. Monte Carlo calculations often must be used to determine the detection efficiency in lieu of actual measurements, though this often can lead to large uncertainties in the cross sections being measured. One method around this threshold-dependent efficiency issue when deuterated scintillators are used is to fit only the recoil-deuteron peak in the light spectrum and assign a corresponding recoil-peak efficiency. Because this method relies on events in a "peak" rather than a continuum, the detection efficiency is now *threshold independent*. Alternately, one can also use the total light spectrum (if unfolded accurately) to obtain another measure of the reaction data to specific states but now using more of the detected events and hence with better statistics.

The total and recoil-peak neutron detection efficiency of the 2×2 detectors were determined using two techinques. The first technique involved the use of the well-known $d(d,n)^3$He cross section [20]. The second technique used the same reaction but in this case the outgoing ^{3}He was measued in coincidence using a silicon surface-barrier ΔE-E detector telescope [21]. The measurements were again conducted at the ND NSL using the FN Van de Graaff accelerator to produce an $E_d = 16$ MeV deuteron beam which impinged on a 2.4 mg/cm^2 deuterated polyethylene target $[C_2D_4]_n$. Recoil-peak efficiency was determined the same way for both cases, but instead of the total light response above a threshold, only the recoil-peak events were included after a suitable computer fit to those peaks [16]. As noted this is *threshold independent.*

The results were compared with a Monte Carlo (MC) calculation using the program MCNP-POLIMI [22]. A MCNP-POLIMI model of the 2×2 detectors was created including the inert gas expansion bubble in the detectors (which results in a slight reduction in overall efficiency and effective solid angle versus a fully loaded 2×2 scintillator). In regard to the recoil-peak efficiency, the differences observed between the present data and Ref. [21] are most likely due to differences in the shape of the peak used to extract the recoil deuteron peak sum. Otherwise, satisfactory agreement is observed between the present [16] and previous measurements [21], and the MC simulations. One can conclude that the use of MCNP-POLIMI to model neutron efficiency for deuterated scintillators over the energy range 1–25 MeV should be sufficient for most (d,n) measurements at least to the 5–10% uncertainty level in efficiency.

III. (d,n) REACTION DATA

A. Specific experimental details

The choice of gaseous and solid targets for the present measurements introduces various neutron transport issues from neutron production in the target to detection of those neutrons by the liquid scintillators outside the scattering chamber. This is important since the neutron spectra are directly determined from unfolding the raw light-response spectra and these must be free of spurious background or corrected for the latter. In these experiments, with the exception of ^{13}C$(d,n)^{14}$N, we are concentrating on measurements to the ground states of the final nuclei to provide a set of systematic spectroscopic data for the g.s. transitions. The relevant g.s. peaks are well above the energies for other events in the light and unfolded spectra and can be reliably measured by several methods. Extraction of data for the excited states is more complicated due to overlapping g.s. spectral data as well as the presence of low-energy break-up deuterons at $E_d = 16$ MeV. Again, except for ^{13}C$(d,n)^{14}$N, excited-state data were deemed less critical as several of the most recent ToF measurements have data for excited states. The published spectroscopic information, often cited in relative units as ZR-DWBA was used, can then be normalized to our absolute g.s. spectroscopic information for a particular final nucleus.

The ground-state and low-lying excited states of the final nuclei are fairly well known and the final ground states are well separated from excited states so these nuclei are well-suited for our purposes. Experimental details and uncertainties for the reactions measured are listed in Table I. [Uncertainties in the solid angles (7.73 millisteradians (msr)) and angular acceptances (5.8°) owing to the finite size of the detectors were deemed negligible compared to the other uncertainties.] Each light spectrum was then postprocessed to extract PSD-gated neutron light spectra. Owing to their size and the volume of liquid scintillator contained, the solid angles of

TABLE I. Experimental details for the (d,n) measurements.

Target	Mean beam energy[a] (MeV)	Lab angular range (deg)	Target thickness (mg/cm^2)
^{9}Be	15.9	10–170	1.85[b]
^{11}B	15.4	10–170	23.1[b]
C_2D_4	15.9	10–170	1.40[b]
^{13}C	15.7	10–170	8.55[b]
^{14}N	15.4	10–170	3.2[c]
^{15}N	15.4	10–170	3.7[c]
^{19}F	15.5	10–170	8.0[c]

[a]Mean beam energy at center of target.
[b]Uncertainty $<+/-5\%$.
[c]Uncertainty $+/-10\%$.

the detectors were determined using Monte Carlo calculations [22]. Solid-target thicknesses were measured with an α gauge, while gaseous targets used the known volume, the measured temperature, and the cell gas pressures that were recorded and monitored throughout an experimental run. Typically, data acquisition time was approximately 30 min per set of angles. The entire set of data for all targets, including extensive back-angle data, could then be measured over a few days as we were using a moderately intense stable beam. Nonetheless this also demonstrates that similar (d,n) measurements (see below) would be feasible using an RIB over the typical 1–2 weeks often used for such experiments [1,5].

B. Light-response spectra

Once the stored event-mode digital waveforms were post-processed, deuteron-recoil events were then gated, and suitable scintillator calibrations applied using γ-source response data to extract light-output spectra in electron-equivalent energy units (MeVee). The individual light-response spectra were then parsed into histograms with 10 keVee bin width from 0.01 to 10 MeVee and stored for inputs into the spectral unfolding code [16]. The latter utilizes accurate response data for EJ315 we have previously measured [16–19].

Figure 2 shows a sample light-response spectrum above threshold (2 MeVee) from the $d + [C_2D_4]_n$ reaction at 10° (lab) and $E_d = 16$ MeV using a 1.4 mg/cm^2 target. The sharp cutoff at 2 MeVee is due to a software threshold applied to the event-mode data.

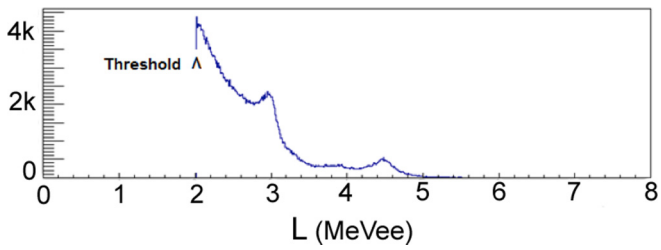

FIG. 2. Light-response spectrum from the $d + [C_2D_4]_n$ reaction at 10° (lab) and incident $E_d = 16$ MeV in electron-equivalent energy units. The software threshold is indicated.

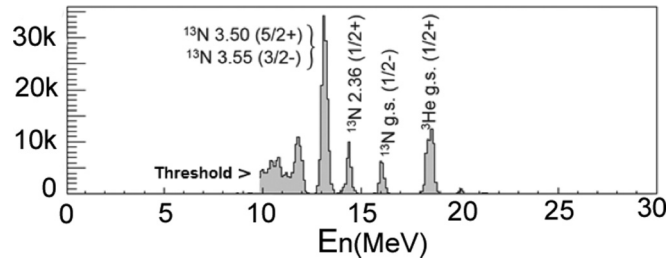

FIG. 3. Unfolded neutron energy spectrum from the $d + [C_2D_4]_n$ reaction at 10° (lab) and incident $E_d = 16$ MeV (Fig. 2). The offline software threshold is indicated.

As previously observed by Brooks and others [6–11], the light-response spectra show broad recoil peaks at discrete neutron energies corresponding to excited levels of the populated final nucleus. An important feature is that lower-energy peaks are "stacked" on top of higher-energy peaks. As an example, if we have two neutron energy groups A and B where $E(A) > E(B)$, we cannot explicitly tell if a neutron came from group A or from group B from the light response data below $E(B)$. However, inspection of each light spectrum versus angle clearly indicates the reaction kinematics producing an appropriate shift in the recoil peak energies with angle. Unlike the present measurements, analysis of previous data taken with deuterated scintillators was limited by the lack of accurate response data and fast computers with efficient unfolding algorithms to extract accurate neutron energy spectra [6–9].

There are two methods that we can employ to obtain cross sections: deuteron-recoil peak fitting from the light spectrum (e.g., Fig. 2) and fitting peaks in an unfolded neutron-energy spectrum (e.g., Fig. 3). The first is a far simpler method but only useful primarily for ground-state peaks (i.e., the highest neutron energy group with little or no underlying background spectrum). The second involves solving the full inverse problem as described in Sec. III C. We first describe the simpler case where we only focus on the ground-state deuteron recoil peak.

In this method the ground-state deuteron recoil peak is fitted with a Gaussian shape, integrated and assigned a recoil-peak efficiency [11,16]. As noted, since we are treating the recoil peak as a Gaussian-like peak, the detection efficiency is *threshold independent* [11,16]. The differential cross section becomes

$$\left(\frac{d\sigma}{d\Omega}\right)_{\text{lab}} = k\frac{N}{\epsilon_p \Omega t I}, \tag{1}$$

where N is the number of observed counts, ϵ_p is the recoil-peak efficiency, Ω is the solid angle, t $(=\rho x)$ is the target areal density, I is the total number of incident beam particles, and k is a constant. Using Eq. (1) and the recoil-peak efficiency, the ground-state cross section from each target is converted to the center-of-mass (c.m.) system. The main uncertainty comes from the recoil-peak efficiency which is estimated at $(+/-10\%)$. The location of the first peak in the differential cross section, which determines the l value of the reaction (Sec. IV), can readily be confirmed without absolute normalization since a comparison is only needed based on

the relative shape. This is in contrast to extraction of spectroscopic factors which requires absolute values for the cross sections.

The ^{9}Be$(d,n)^{10}$B reaction has been previously measured at $E_d = 16$ MeV [23] and conveniently provides a direct comparison of the deuteron-recoil peak-fitting method to the traditional long-path n-ToF method. Very good agreement with the data of Ref. [23] is observed [11,16] and demonstrates the simplicity and reliability of this method. Prior to having accurate detector response data, we previously reported transfer cross sections extracted using the above method [9–11]. However, better statistics are obtained if the full unfolded spectral data can be used (see below). The recoil-peak data can still be used to provide a check on the cross sections extracted from the unfolding procedure and this was done here.

With the exception of some nuclear astrophysics problems and many RIB studies, ground-state cross sections alone are often of limited interest without at least low-lying excited states included. One then needs to rely on spectrum unfolding techniques with accurately known response functions to extract reliable neutron energy spectra from the raw light-response spectra, assuming the latter are relatively free of background neutrons. This is described in more detail elsewhere for the detectors used in this experiment [16–19]. As noted, unfolded spectra now include a threshold-dependent intrinsic detection efficiency but have much better statistics (typically $\times$ 4). The uncertainty propagation in neutron spectrum unfolding methods is still not well understood [24,25]. Approximations used for the uncertainty in the unfolded result are discussed below in extraction of the spectroscopic factors (see also [16]).

C. Unfolded neutron energy spectra

Unfolding results for the $d + [C_2D_4]_n$ reaction (Fig. 2) at 10° (lab) are shown in Fig. 3. The unfolding software [16] uses the maximum-likelihood estimation method (MLEM). The ground states of ^{3}He, ^{13}N, and excited states of ^{13}N are clearly seen, with reasonably good resolution for a neutron measurement. However the $E_x = 3.50$ and 3.55 MeV states of ^{13}N are not separated and instead a prominent peak consisting of the two levels is observed (Fig. 3). The proton separation energy for ^{13}N is $S_p = 1.943$ MeV and thus the excited states in ^{13}N observed are proton unbound. These are important data as they demonstrate the spectroscopic capability of the UM-DSA array for the study of particle-unbound states, which will become more relevant in the transition to experiments involving RIBs. The lifetimes of the states observed correspond to decay widths of $\Gamma = 31.7$, 62, and 47 keV, respectively (ENDF/B-VII.0). The $d(d,n)^{3}$He cross section was determined at 10, 15, 30, and 130° (lab) by integration of the ^{3}He ground-state peak. Since the $d(d,n)^{3}$He cross section is well known, as discussed earlier, the detection efficiency was then determined by comparing the ratio of the uncorrected measured cross section with published data.

The unfolding procedure for the other targets followed the recipe used for the $d + [C_2D_4]_n$ spectra. The threshold was typically set at 2 MeVee in software with the exception

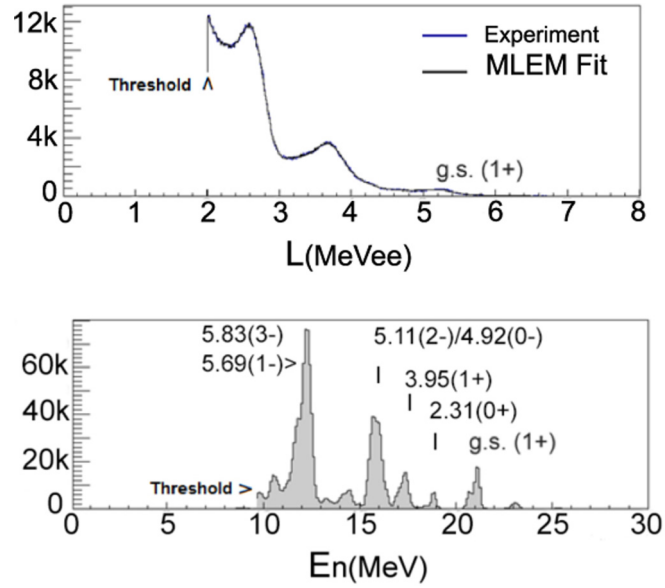

FIG. 4. Light-response spectrum (top) and unfolded neutron energy spectrum (bottom) from the ^{13}C$(d,n)^{14}$N reaction at 20° (lab) and $E_d = 16$ MeV. The offline software threshold is indicated. Known states in ^{14}N are indicated by their excitation energy, spin, and parity (see text).

of the $d + SF_6$ spectra beyond 90° (lab) which has slightly poorer deuteron-proton separation and required a threshold of 2.5 MeVee. Figure 4 shows the raw light-response spectrum and unfolded neutron spectrum from the ^{13}C$(d,n)^{14}$N reaction at 20° (lab) with the ^{14}N ground state and some known excited states labeled. The jagged line in the light-response spectrum represents the raw data and the overlapping smooth line corresponds to the MLEM estimate after 5000 iterations. The fit between the MLEM estimate and the raw light response spectrum is excellent, indicating the response matrix describes well the spectral response and that the data are devoid of most background neutrons. Note that a small spurious peak appears at $E_n = \sim$23 MeV just beyond the calculated ^{14}N ground-state peak location. Further investigation shows that this is due to recoil protons which leak into the deuteron PSD gate due to breakup of scintillator deuterons [10,11,14–16]. The overall effect is small but can add to the systematic uncertainty of the measurements.

In a recent experiment at $E_d = 6$ MeV evaluating an improved deuterated liquid scintillator (EJ301D), we obtained a ^{13}C(d,n) spectrum devoid of such spurious peaks and with somewhat better resolution [15]. The forward angle data closely resemble the data obtained in this experiment (Fig. 4). As noted, several of the ^{14}N states seen in these measurements are important in nuclear astrophysics and will be discussed in Sec. IV D.

Spectrum unfolding results for the ^{14}N$(d,n)^{15}$O reaction at 5° (lab) are shown in Fig. 5. The ground state and $E_x = 6.17$ MeV excited state are labeled. As with the ^{13}C$(d,n)^{14}$N unfolding results, the MLEM fit also describes very well the spectral shape of the light-response spectrum. An interesting feature that is present in all three unfolding results shown

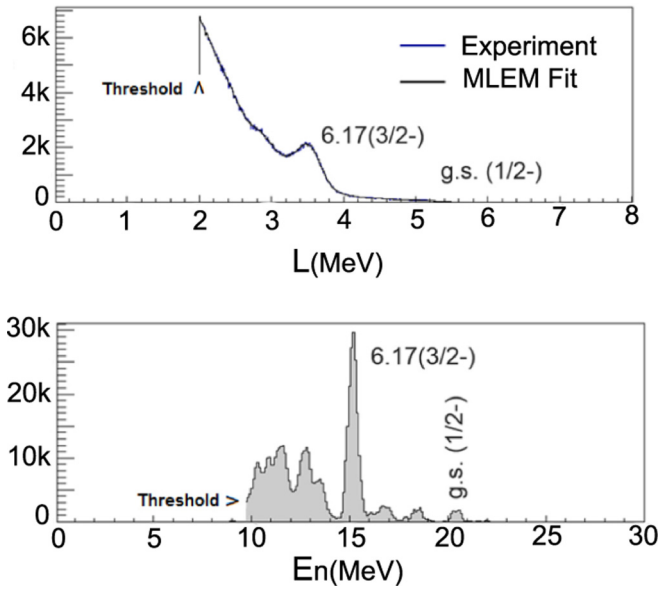

FIG. 5. Light-response spectrum (top) and unfolded neutron energy spectrum (bottom) from the ^{14}N$(d,n)^{15}$O reaction at 5° (lab) and incident $E_d = 16$ MeV. The offline software threshold is indicated.

is the rich amount of information that is extracted by the MLEM unfolding from the raw light response. By eye, one can identify only the strongly populated levels from the latter but the spectrum unfolding technique appears capable of reliably extracting many more details in the incident neutron spectra than obvious from the raw light-response spectra. The effective energy resolution is often better than a typical n-ToF measurement using a modest flight path for $E_n > 10$ MeV [23]. This is true if the deuterated scintillator data is devoid of most background and the PSD can separate the recoil deuterons cleanly over a range of energies [10,11,14–16]. In many of the nuclei studied, this is still not sufficient to adequately resolve many of the individual excited states. Hence for this and other reasons (see below) with the exception of the ^{13}C target, we concentrate on analysis of data to the ground states of the final nuclei.

D. Differential cross sections from unfolded spectra

Once the unfolded neutron spectra are obtained, the differential cross section can be determined [Eq. (1)], with the total number of incident deuterons calculated from the integrated beam current on the downstream Faraday cup. Recall that the threshold-dependent efficiency is included as an output of the MLEM spectral unfolding code. This is quite convenient as one can adjust the MLEM threshold to yield convergence and the efficiency is then determined. The differential cross sections obtained in this manner, together with the related published elastic deuteron scattering data, are shown in Figs. 6–12. The (d,n) g.s. data shown agree within the uncertainties (typically $+/-10\%$) with those obtained from the deuteron recoil-peak method [11,16] described earlier.

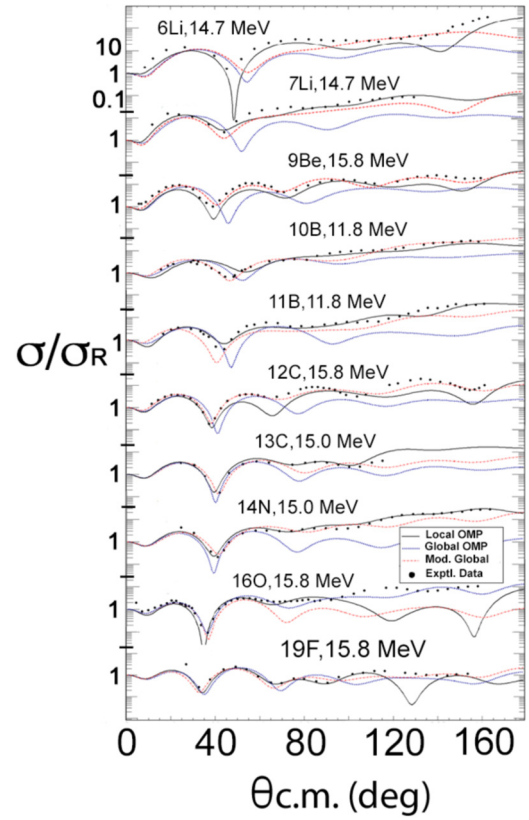

FIG. 6. Deuteron elastic scattering optical-model calculations (using global, modified global, and local OMPs compared with various published (d,d) elastic scattering data sets [16], displayed as ratio to Rutherford scattering.

IV. REACTION ANALYSIS

A. (d,n) proton-transfer selection rules

The angular distributions for (d,n) reactions such as those measured here, which are well above the Coulomb barrier, contain a rich amount of information regarding the transfer

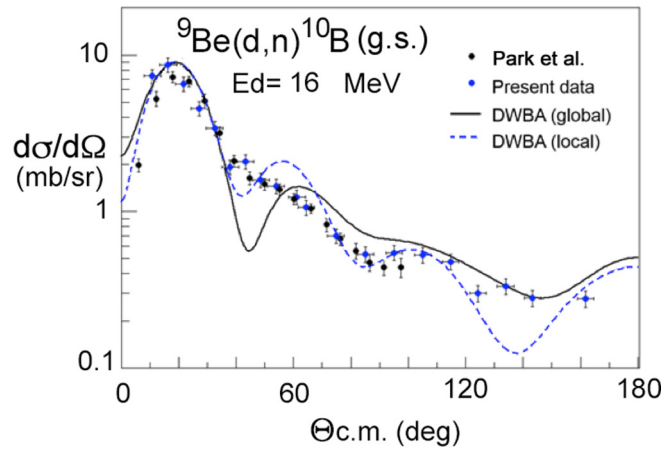

FIG. 7. Measured ^{9}Be$(d,n)^{10}$B(g.s.) cross section compared to the n-ToF data of Park *et al.*, from 1973 [23]. FR-DWBA calculations with global and local OMPs also are shown.

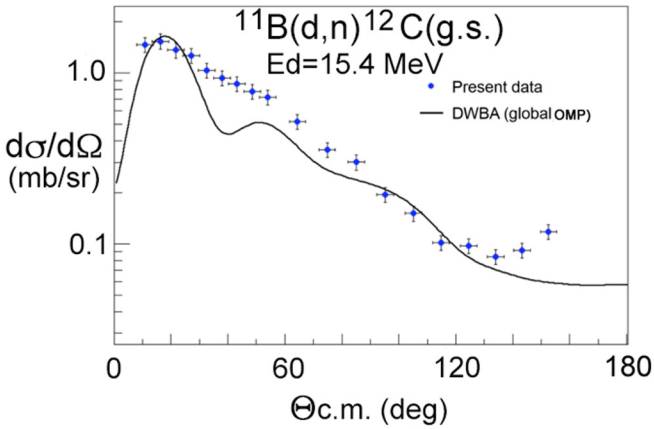

FIG. 8. Measured ^{11}B$(d,n)^{12}$C(g.s.) cross sections compared with a FR-DWBA calculation using global OMPs.

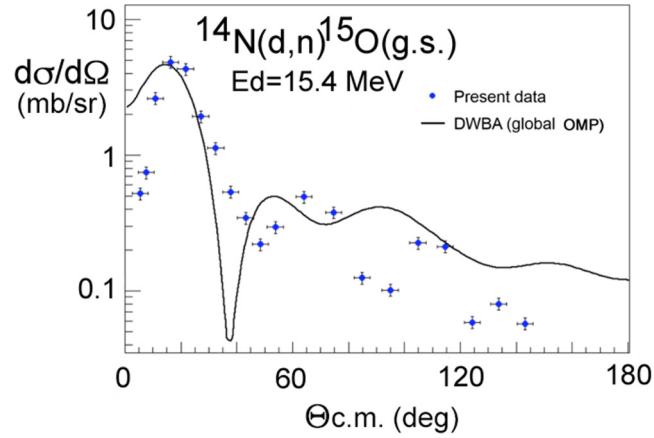

FIG. 10. Measured ^{14}N$(d,n)^{15}$O(g.s.) differential cross sections compared with a FR-DWBA calculation using global OMPs.

reaction. Thus as well known, an accurate (d,n) measurement covering a number of forward angles can set a limit on the spin and parity of a given final state [26–28], as often desired in studying RIB reactions leading to exotic nuclei far from stability. In addition, data taken at back angles, which is often limited using n-ToF, can verify if the reaction is primarily a direct reaction, as assumed above and as needed for a valid DWBA analysis to extract spectroscopic information and especially for FR-DWBA analysis [26–28].

Since the present measurements involve final states and single-particle levels where the spins and other information are known, the angular momentum transfers needed for the reaction analysis are *a priori* specified.

B. Distorted-wave Born approximation (DWBA)

The distorted-wave Born approximation (DWBA) has been successfully applied to single-nucleon transfer reactions including (d,p) and (d,n) reactions, as well as inelastic scattering [26–29]. A key requirement is to describe the incident and outgoing projectile channels with a uniform set of optical-model scattering potentials.

1. *Optical-model potentials (OMPs)*

We use an empirical complex optical model fit to published experimental data from elastic scattering measurements for nuclei $A < 20$ in the energy range of our data ($E_d = 16$ MeV). The latter were obtained on a case-by-case basis by various authors or on a global basis by analyzing a wide set of data (e.g., [30–33]). The latter type of potentials give an overall representation of the OMPs in a given mass region and are usually preferred to obtain systematics for spectroscopic information over a range of nuclei.

The distorting potentials are of the form

$$U(\vec{r}) = U_c(\vec{r}) + U_{OM}(\vec{r}), \tag{2}$$

where $U_c(\vec{r})$ is the Coulomb potential due to a uniformly charged sphere of radius R_c and $U_{OM}(\vec{r})$ is the complex optical-model potential. The latter consists of conventional complex Wood-Saxon volume and surface potentials together with a derivative spin-orbit potential [26–28,30–33].

2. *Spectroscopic factors and strengths*

The DWBA transition amplitude for (d,n) assumes the reaction is a direct proton stripping to a single final particle

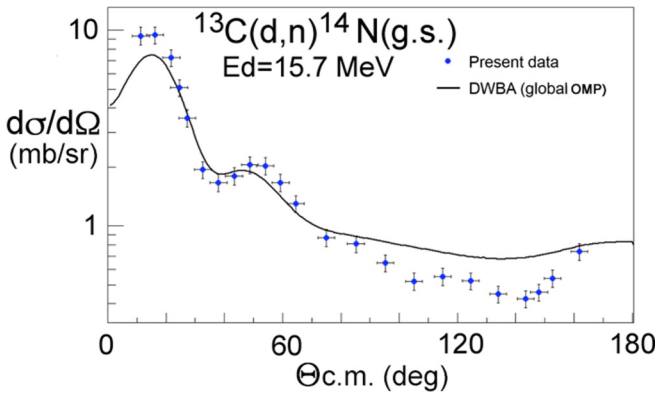

FIG. 9. Measured ^{13}C$(d,n)^{12}$N(g.s.) differential cross sections compared with a FR-DWBA calculation using global OMPs.

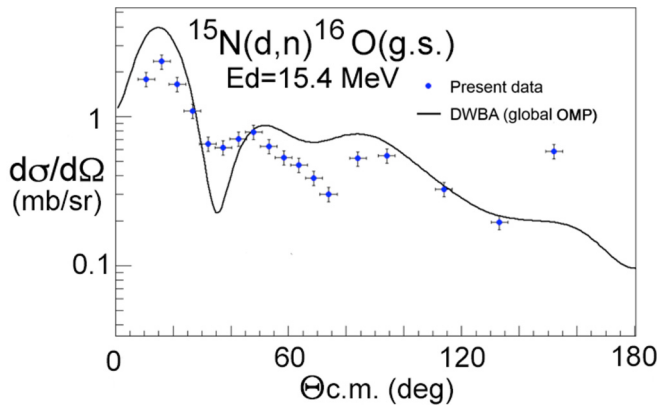

FIG. 11. Measured ^{15}N$(d,n)^{16}$O(g.s.) differential cross section compared with a FR-DWBA calculation using global OMPs.

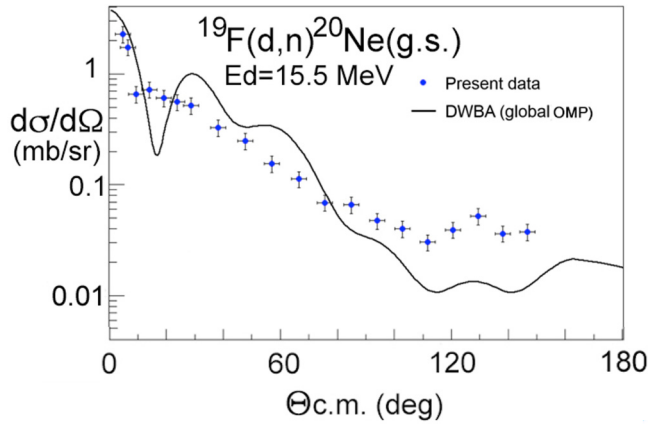

FIG. 12. Measured ^{19}F$(d,n)^{20}$Ne(g.s.) differential cross sections compared with a FR-DWBA calculation using global OMPs.

state. In reality, this is complicated by residual interactions that may lead to configuration mixing of states with the same angular momentum and parity. Deviations from a pure single-particle state can then be described by the *spectroscopic factor* ($\mathcal{S}F$),

$$\left(\frac{d\sigma}{d\Omega}\right)_{\text{expt}} = \frac{2J_f+1}{2J_i+1}\mathcal{S}F\left(\frac{d\sigma}{d\Omega}\right)_{\text{DWBA}}. \tag{3}$$

If the final spin is unknown, the spectroscopic factor can be written as the *spectroscopic strength* $\mathcal{S}$ which includes the initial and final state angular momentum terms:

$$\mathcal{S} = \frac{2J_f+1}{2J_i+1}\,\mathcal{S}F \tag{4}$$

and hence

$$\left(\frac{d\sigma}{d\Omega}\right)_{\text{expt}} = \mathcal{S}\left(\frac{d\sigma}{d\Omega}\right)_{\text{DWBA}}. \tag{5}$$

The shape of the differential cross section is related to the angular momentum transfer of the reaction [26–29]. As noted, for the systematic extraction of spectroscopic factors over a mass range, it is preferable that one uses global OMPs rather than local potentials as the former represent an average trend over a mass region rather than an individual fit to specific nuclei. Many global potentials exist for protons, neutrons, and deuterons for nuclei $A > 40$ covering a broad mass and energy range [30–33]. To explicitly show this effect, Fig. 6 displays a comparison of deuteron elastic scattering data with calculations using local OMPs, and the Daehnick global OMP [32] which is valid for $A \geqslant 27$. After careful evaluation, it was determined that the major deviations are due to an overprediction of the absorptive (imaginary) surface potential. Figure 6 also contains calculations using a modified Daehnick potential where the code SFresco [34] was used to adjust the imaginary surface OMP term to improve the fits. A list of the alternate, local deuteron optical model parameters used in the analysis is tabulated in Ref. [16].

The modified global potential is adequate in reproducing the elastic scattering to about 30° which is an important region for extraction of spectroscopic factors at bombarding energies well above the Coulomb barrier as is the case here (incident $E_d = 16$ MeV). Beyond 30°, deviations are observed. No apparent trend was readily found in the SFresco fits but on average the global imaginary surface term appears to be ∼30% higher than the value determined from the individual fits.

Calculations were performed using the finite-range DWBA codes Fresco ([34], with a special GUI interface added to expedite the calculations [16]), and Ptolemy [35]. The unmodified deuteron global potential of Daehnick *et al.* [32] was used for analysis of the individual (d,n) reactions studied in this work as the deuteron elastic scattering at forward angles is adequately reproduced (Fig. 6). Calculations using other OMPs including the modified global OMPs were then used to estimate the uncertainties in the spectroscopic information extracted from the FR-DWBA calculations due to uncertainties in the OMPs.

The Chapel Hill 89 (CH89) global potential [31] was the primary potential used for the neutron exit channel. For the proton-core potential, a Woods-Saxon shape was used with $r_o = 1.25$ fm and $a = 0.65$ fm. The well depth was adjusted to reproduce the single-proton binding energy (S_p). A spin-orbit potential also was included with the same r_o and a_o, with $V_{so} = 7.0$ MeV. We used a bound-state proton potential commonly adopted by others for earlier analyses of (d,n) reactions as this then permits a comparison of spectroscopic factors extracted since the latter can depend on the particular bound-state wave function used in the DWBA calculations [36–40].

The measured differential cross section and FR-DWBA calculations for ^{9}Be$(d,n)^{10}$B are shown in Fig. 7, where E_d is the deuteron energy at the center of target. The ground state of ^{10}B is $J^\pi = 3^+$ and for ^{9}Be $J^\pi = \frac{3}{2}^-$, thus the change in parity constrains ℓ to odd values. Indeed from Fig. 7, the DWBA calculation with $\ell = 1$ matches the first peak at ∼20°. The ^{9}Be$(d,n)^{10}$B reaction has been measured near $E_d = 16$ MeV [23] and thus a direct comparison to that n-ToF data can be made. This is shown in Fig. 7, with the good agreement noted verifying the validity of using deuterated scintillators and the related unfolding methods for this type of measurement. FR-DWBA calculations using both global and local [23] OMPs also are shown in Fig. 7.

Our data extend to larger angles and indicates the possible presence of contributions from nondirect reaction mechanisms, such as neutron emission from a compound nucleus, that tend to be less forward-peaked [34]. Such contributions can also smooth out some of the structure at forward angles, e.g., the minimum near 40° shown in Fig. 7, which is difficult to fit with conventional DWBA.

The measured differential cross section for ^{11}B$(d,n)^{12}$C is shown in Fig. 8. As with ^{9}Be$(d,n)^{10}$C, the change in parity constrains possible ℓ values to odd values which agrees with the DWBA calculation with $\ell = 1$. The DWBA calculation does not fit the shape of the differential cross section very well but does match the overall trend of the differential cross section. Similar conclusions were made for data measured at $E_d = 6$ MeV [36]. The increase in cross sections near 140° could again be due to nondirect cross section contributions, or the fact that ^{12}C in a simple αcluster model is deformed and there could be coupling to excited states. This could then

affect the relatively low cross sections observed at forward angles, e.g., smoothing out the minima in the direct-transfer differential cross section [34].

The ^{13}C(d,n)^{14}N and ^{14}N(d,n)^{15}O differential cross sections are shown in Figs. 9 and 10. The DWBA calculations agree with the data at forward angles for the expected $\ell = 1$ transfers. The DWBA calculation poorly describes the complete shape of the data for ^{14}N(d,n)^{15}O at back angles but is much better in the case of ^{13}C(d,n)^{14}N. In all the cases shown, improvements are likely possible with more advanced forms of analysis such as adiabatic deuteron breakup approximations, coupling to strongly populated states, pre-equilibrium neutron emission, etc. [26–28,34]. That level of analysis should not be needed to extract useful spectroscopic information from the large cross section forward-angle data (<60°) where DWBA adequately describes the cross sections in most cases. However, our data using deuterated scintillators provide cross sections over a wide angular range to permit a more complex reaction analysis if deemed appropriate.

In the case of ^{13}C(d,n) we observe several low-lying resolved states in ^{14}N at $E_x = 2.31$ and 3.95 MeV that have significance in nuclear astrophysics. In particular, the proton-stripping spectroscopic factors and reduced widths for these levels can be used in the calculations of cross sections for radiative proton capture on ^{13}C [2,4]. Recent attempts to do this using data from the (^{3}He,d) reaction had issues [41] with the information extracted for the $E_x = 2.31$ MeV state (Fig. 4) and the latter data could not be used.

Differential cross section for the ^{15}N(d,n)^{16}O and ^{19}F(d,n)^{20}Ne reactions are shown in Figs. 11 and 12. As expected, both cross sections mostly agree at forward angles with FR-DWBA calculations for the expected $\ell = 1$ and $\ell = 0$ transfers, respectively. The nucleus ^{19}F is known to be deformed and FR-DWBA using coupled channels would be more realistic [34]. This would tend to smooth out the angular distribution and likewise contribute to the data at large angles [40].

C. Spectroscopic factors

The spectroscopic factors for each target were extracted by fitting the data points from approximately 0–60° degrees c.m. This choice of angular range was based on the FR-DWBA and global OMP trends shown in the previous figures. In the present measurements the deduced spectroscopic factors have an uncertainty estimated to be ±15% arising mainly from the uncertainty in neutron detection efficiency, the spectrum unfolding (MLEM) procedure, the uncertainty in FR-DWBA calculations (e.g., from the use of various OMPs), and uncertainties in fitting the experimental data (Figs. 8–13.) The relative uncertainty, removing the uncertainty in detection efficiency that is a systematic effect, is somewhat less than this (approximately ±12%)

The results are reported in Table II. Where data exist at 16.0 MeV [23], the results using a local OMP are also included in addition to those using the global OMPs. Again, the ^{9}Be(d,n)^{10}B reaction provides a direct comparison with published n-ToF results (Fig. 7) at the same incident energy. The ^{10}B ground-state spectroscopic factor deduced using the local OMP of [23] shows good agreement with the spectroscopic factor reported by those authors. In contrast, the spectroscopic factors deduced from our measurements are lower by about a factor of 2 for the ^{11}B, ^{13}C(d,n)^{12}C, ^{14}N measurements done at 11.8 MeV reported in Ref. [37]. However this is not a surprise since the analysis in Ref. [37] was done with ZR-DWBA (see below).

It also should be noted that most of the n-ToF and other measurements were done many decades ago, and again most analyzed using zero-range DWBA, i.e., assuming the deuteron is a point particle. Unlike FR-DWBA which is an absolute cross-section calculation, the previous ZR-DWBA calculations often use a semiempirical normalization factor to extract spectroscopic factors [23,37]. It is somewhat surprising that a number of the earlier (d,n) results generally agree with our 16 MeV data and the corresponding FR-DWBA analyses. The exceptions are for the closed-shell final nucleus ^{16}O and to some extent ^{12}C and ^{14}N final nuclei which yield lower spectroscopic factors in our analysis at $E_d = 16$ MeV. However, analysis of (d,n) measurements done at relatively low energies and many of the (^{3}He,d) measurements for these nuclei show wide variations in the published spectroscopic information (e.g., see the tables in the references cited in Table II).

Cohen and Kurath (CK [42]) have calculated spectroscopic factors expected from the nuclear shell model for many of the nuclei listed in Table II. Again their calculations use the same

TABLE II. Spectroscopic factors.

Final nucleus	J^π, T	nlj	ℓ_p	Present work[a]		Previous measurements		Ref.	SM[b]
				global	local	(dn)	E_d (MeV)		
^{10}B	3$^+$, 0	1$p_{3/2}$	1	1.21	1.35	1.33	16.0	[23]	1.20
^{12}C	0$^+$, 0	1$p_{3/2}$	1	3.58		4.18	11.8	[37]	5.70
^{14}N	1$^+$, 0	1$p_{1/2}$	1	1.17	1.04	2.18	11.8	[37]	1.38, 1.20
	0+,1	1$p_{3/2}$	1	0.74	0.70	2.48	"	"	1.73, 1.39
	1+,0	1$p_{3/2}$	1	0.62	0.53	0.82	"	"	
^{15}O	$^1/_2^-$, $^1/_2$	1$p_{1/2}$	1	1.11		1.00	6.0	[38]	1.25, 1.42
^{16}O	0$^+$, 0	1$p_{1/2}$	1	2.63		3.7	6.0	[39]	n.a.
^{20}Ne	0$^+$, 0	2$s_{1/2}$	0	0.45		0.4	6.5	[40]	n.a.

[a]Estimated uncertainty is ±15%. Unless otherwise noted, transitions are to ground states.
[b]Shell-model calculations of Cohen-Kurath [42] and Varma-Goldhammer [43], respectively.

proton potential-well geometry parameters as we and many others have used in ZR-DWBA or FR-DWBA calculations. Hence a comparison of the experimental and CK spectroscopic factors should be valid. A few years later, such calculations were updated by Varma and Goldhammer (VG [43]). Except for the ^{12}C g.s. both shell-model calculations agree with our g.s. measurements within our uncertainties. Our and others' (d,n) spectroscopic factors for the tightly bound ^{12}C g.s. are noticeably smaller and this may also apply to the doubly magic nucleus ^{16}O g.s. (Table II) but CK and VG do not include ^{16}O in their calculations. Also as noted, the ^{12}C g.s. is deformed.

A reduction (i.e., quenching) in spectroscopic factors is observed in nucleon knockout reactions and is attributed to strong nucleon-nucleon correlations in such nuclei [44,45]. We do not see that effect for most of the nuclei studied here with (d,n), but it may contribute to reduced spectroscopic factors for the more tightly bound nuclei ^{12}C and ^{16}O (Table II).

D. ^{13}C$(d,n)^{14}$N spectroscopy for nuclear astrophysics

The reaction ^{13}C$(d,n)^{14}$N is of particular interest in nuclear astrophysics as the spectroscopic information obtained for the lowest excited states in ^{14}N, which are resolved in the present experiment (Fig. 4), can provide important information for accurate calculation of the radiative proton capture [2,4,41] on ^{13}C. As noted, attempts to use the $(^3$He$,d)$ reaction for this had difficulties related to the anomalous population of the 2.31 MeV level in ^{14}N [41]. Our data at $E_d = 16$ and 6 MeV [15] as well as earlier (d,n) measurements [37] appear to be consistent between different bombarding energies.

In Table II we display the spectroscopic factors we have extracted for the low-lying states in ^{14}N with FR-DWBA using both global and local OMPs, and compare these with two shell-model (SM) calculations. As noted for the g.s. value, the spectroscopic values observed for the excited states noted are close to those expected from the nuclear shell model, and in particular the later calculations of [43], although our value for the 2.31 MeV level is somewhat lower than expected. This and the other results shown in Table II give support for the use of (d,n) to deduce useful spectroscopic data for astrophysics calculations, and deuterated scintillators have many advantages for such measurements.

E. Feasibility study: RIB reaction ^{7}Be$(d,n)^{8}$B

In addition to the above stable-beam (d,n) measurements, the UM-DSA array was also used to obtain preliminary data for the radioactive ion beam (RIB)-induced ^{7}Be$(d,n)^{8}$B reaction done using inverse kinematics (i.e., ^{7}Be beam on deuterons). This is an important reaction to understand for the generation of solar neutrinos and other problems in nuclear astrophysics [2,4]. A previous measurement involved the detection of the ^{8}B recoil in a fairly high background and was limited mostly to forward angles [46]. The present RIB experiment [16] was carried out at the *TwinSol* RIB facility [5] at the ND NSL FN tandem laboratory. It was done to test the feasibility of using the UM-DSA detectors for low-energy RIB or measurements involving the detection of neutrons.

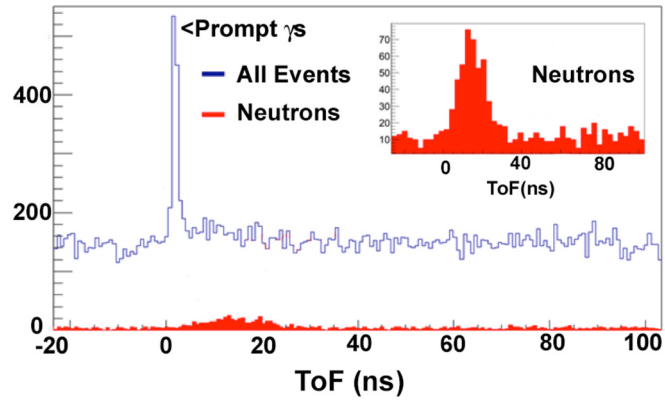

FIG. 13. DSP-gated UM-DSA $d(^{7}$Be$,n)^{8}$B short-path n-ToF spectrum showing summed (d,n) events near 90° (lab), $E(^{7}$Be$) =$ 30 MeV.

This experiment like many using RIBs was done as noted in inverse kinematics, here with a low-intensity (10^5/s–10^6/s) secondary ^{7}Be beam, $E =$ approximately 30 MeV incident on a CD_2 target. Approximately 120 h of data were collected over 6 days. Signals were taken in coincidence with a ^{8}B recoil detector and used short-path n-ToF (Fig. 1) to further suppress the intense prompt γ flash.

A short-path n-ToF plot is shown in Fig. 13, with all scintillator events near 90° (lab) shown together with the PSD-gated deuteron recoil events [16]. Although the limited cross sections deduced appear compatible with those reported in Ref. [46], it is obvious that further measurements are not possible without good PSD to better separate low-energy γ rays and neutrons. In particular, when done at low bombarding energy with inverse kinematics the outgoing neutrons at many angles will be emitted at *very* low energies ($E_n < 2$ MeV). The present PSD using EJ315 and similar liquid scintillators is marginal at those energies. While coincidence with a nuclear recoil particle (as in the present study) helps in this regard, improvements in PSD are needed to better pursue this and similar experiments further. Thus, we have recently developed a new deuterated-scintillator (d-xylene, EJ301D; [15,47–49]) with somewhat improved PSD. We are pursuing development of other types of deuterated liquid and crystalline scintillators to permit (d,n) and similar measurements using low-energy stable beams and RIBs [47,49].

V. SUMMARY

The use of a deuterated liquid-scintillator array (UM-DSA) for obtaining systematic spectroscopy information from the (d,n) reaction at $E_d = 16$ MeV without the use of long-path n-ToF has been demonstrated for a range of nuclei, $A < 20$. The ^{9}Be(d,n) data agree well with a previous measurement at $E_d = 16$ MeV using long-path n-ToF. This demonstrates the ability to measure neutron cross sections with such an array even when long-path n-ToF is not feasible as now also demonstrated in a variety of other experiments by our group and others [8–19]. The MLEM spectral-unfolding method is shown to provide a reliable tool for neutron-spectrum unfolding when an accurate response matrix is available.

Spectroscopic information of astrophysics interest was obtained from analysis of the $^{13}C(d,n)$ reaction data to low-lying excited states in ^{14}N. However, improvements in PSD are needed, e.g., including development of new types of deuterated scintillators, to better pursue measurements involving low energy neutrons, e.g., $E_n < 2$ MeV [15,47–49].

ACKNOWLEDGMENTS

Much of the material presented in this paper is based on work done as a UM Ph.D. thesis by the lead author [16]. Details on the UM-DSA array, the early data obtained, and the unfolding procedures have been presented by one or more of the authors in several of the journal articles and conference proceedings cited in the text. We thank our collaborators at UM, UND, Ohio University, and ORNL for their assistance in various aspects of this and related work. The (d,n) measurements and analyses reported here were supported in part by the US National Science Foundation (Grants No. NSF PHY14-01242, No. NSF PHY14-01343, and related, earlier grants).

[1] D. W. Bardayan *et al.*, Recent Astrophysical Measurements Using the *TwinSol* Separator, J. Phys. Conf. Ser. **730**, 012004 (2016).

[2] R. N. Boyd, *An Introduction to Nuclear Astrophysics* (The University of Chicago Press, Chicago,2008).

[3] S. Kubono *et al.*, Determination of the Sub-Threshold State Contribution in $^{13}C(\alpha,n)^{16}O$, the Main Neutron-Source Reaction for the s Process, Phys. Rev. Lett. **90**, 062501 (2003).

[4] D. W. Bardayan, Recent Experimental progress in nuclear astrophysics, Phys. Proc. **66**, 457 (2015).

[5] F. D. Becchetti and J. J. Kolata, Recent results from the TwinSol low-energy RIB facility, Nucl. Instrum. Methods Phys. Res. B **376**, 397 (2016).

[6] F. D. Brooks, Development of Organic Scintillators, Nucl. Instrum. Methods **162**, 477 (1979); F. D. Brooks, W. A. Cilliers, B. R. S. Simson, F. D. Smit, M. S. Allie, D. T. L. Jones, W. R. McMurray, and J. V. Pilcher, Deuterated anthracene spectrometer for 5−30 MeV neutrons, Nucl. Instrum. Methods A **270**, 149 (1988).

[7] F. D. Brooks, P. M. Lister, J. M. Nelson, and K. S. Dhuga, Vector analyzing powers for the $^{12}C(d,n)^{13}N$, $^{9}Be(d,n)^{10}B$, and $^{28}Si(d,n)^{29}P$ reactions, *5th International Symposium on Polarization Phenomena in Nuclear Physics*, edited by G. G. Ohlsen, R. E. Brown, N. Jarmie, W. W. McNaughton, and G. M. Hale, AIP Conf. Proc. No. 69 (AIP, Santa Fe, 1981), p. 656.

[8] M. Ojaruega, Fast Neutron Measurements using Deuterated Liquid Scintillators, Ph.D. thesis, The University of Michigan, 2009; http://research.physics.lsa.umich.edu/twinsol/Publications/publications.html

[9] M. Ojaruega, F. D. Becchetti, A. N. Villano, H. Jiang, R. O. Torres-Isea, J. J. Kolata, A. Roberts, and C. C. Lawrence, Evaluation of large deuterated scintillators for fast neutron detection ($E = 0.5$−20 MeV) using the $D(d,n)^3He$, $^{13}C(d,n)$ and $^{27}Al(d,n)$ reactions, Nucl. Instrum. Methods Phys. Res. A **652**, 397 (2011).

[10] M. Febbraro, F. D. Becchetti, R. O. Torres-Isea, M. Ojaruega, A. M. Howard, J. J.Kolata, A. Roberts, and A. N. Villano, Neutron spectroscopy without time-of-flight measurement: A DSP-based deuterated scintillator array, IEEE Trans. Nucl. Sci. **60**, 890 (2013).

[11] M. Febbraro, F. D. Becchetti, R. O. Torres-Isea, A. M. Howard, A. Riggins, C. Lawrence, and J. J. Kolata, Systematic study of (d,n) reactions at $E_d = 16$ MeV using a deuterated scintillator array, EPJ Web Conf. **66**, 03026 (2014).

[12] V. Bildstein, P. E.Garrett, J. Wong *et al.*, Comparison of deuterated and normal liquid scintillators for fast-neutron detection, Nucl. Instrum. Methods Phys. Res. A **729**, 188 (2013).

[13] P. E. Garrett, DESCANT – the deuterated scintillator array for neutron tagging, Hyperfine Interact. **225**, 137 (2013).

[14] M. Febbraro, C. C. Lawrence, H. Zhu, B. Pierson, R. Torres-Isea, F. D. Becchetti, J. J. Kolata, and J. Riggins, Deuterated scintillators and their application to neutron spectroscopy, Nucl. Instrum. Methods Phys. Res. A **784**, 184 (2015).

[15] F. D. Becchetti, R. S. Raymond, R. O. Torres-Isea, A. Di Fulvio, S. D. Clarke, S. A. Pozzi, and M. Febbraro, Deuterated -xylene (xylene-d10; EJ301D): A new, improved deuterated liquid scintillator for neutron energy measurements without time-of-flight, Nucl. Instrum. Methods Phys. Res. A **820**, 112 (2016).

[16] M. T. Febbraro, A Deuterated Neutron Detector Array for the Study of Nuclear Reactions with Stable and Rare Isotope Beams, Ph.D. thesis, The University of Michigan, 2014; http://research.physics.lsa.umich.edu/twinsol/Publications/publications.html

[17] C. C. Lawrence, Neutron Spectrum Unfolding with Organic Scintillators for Arms-control Verification, Ph.D. thesis, The University of Michigan, 2014; http://research.physics.lsa.umich.edu/twinsol/Publications/publications.html

[18] C. C. Lawrence, A. Enqvist, M. Flaska, S. A. Pozzi, A. M. Howard, J. J. Kolata, and F. D. Becchetti, Response characterization for an EJ315 deuterated organic-liquid scintillation detector for neutron spectroscopy, Nucl. Instrum. Methods Phys. Res. A **727**, 21 (2013). (Note: The fourth level in the ^{14}N spectrum shown is mislabeled as a $J^\pi = 1^-$).

[19] C. C. Lawrence, A. Enqvist, M. Flaska, S. A. Pozzi, and F. D. Becchetti, Comparison of spectrum -unfolding performance of (EJ315) and (EJ309) liquid scintillators on measured 252Cf pulse-height spectra, Nucl. Instrum. Methods Phys. Res. A **729**, 924 (2013).

[20] F. S. Dietrich, E. G. Adelberger, and W. E. Meyerhof, Study of the $^2H(d,n)^3He$ reaction between 12 and 19 MeV, Nucl. Phys. A **184**, 449 (1972).

[21] A. N. Villano, F. D. Becchetti, J. J. Kolata, M. Ojaruega, and A. Roberts, Efficiency measurements of deuterated liquid scintillators using $d(d,n)^3He$ coincidence events, Nucl. Instrum. Methods Phys. Res. A **652**, 280 (2011).

[22] S. A. Pozzi, E. Padovani, and M. Marseguerra, MCPN-PoliMi: A Monte Carlo code for correlation measurements, Nucl. Instrum. Methods Phys. Res. A **513**, 550 (2003).

[23] Y. S. Park, A. Niiler, and R. A. Lindgren, Spectroscopy of ^{10}B from $^{9}Be(d,n)^{10}B$ Reaction, Phys. Rev. C **8**, 1557 (1973).

[24] Marcel Reginatto, Paul Goldhagen, and Sonja Neumann, Spectrum unfolding, sensitivity analysis and propagation of uncertainties with maximum entropy deconvolution code MAXED, Nucl. Instrum. Methods Phys. Res. A **476**, 242 (2002).

[25] M. Matzke, Propagation of uncertainties in unfolding procedures, Nucl. Instrum. Methods Phys. Res. A **476**, 230 (2002).
[26] C. A. Bertulani and P. Danielewicz, *Introduction to Nuclear Reactions* (IOP, Bristol, 2004).
[27] G. R. Satchler, *Direct Nuclear Reactions*, International Series of Monographs on Physics No. 68 (Oxford University Press, Oxford,1983).
[28] N. K. Glendenning, *Direct Nuclear Reactions* (World Scientific, Singapore, 2004).
[29] L. L. Lee, Jr., J. P. Schiffer, B. Zeidman, G. R. Satchler, R. M. Drisko, and R. H. Bassel, ^{40}Ca$(d,p)^{41}$Ca, a test of the validity of the distorted-wave born approximation, Phys. Rev. **136**, B971 (1964).
[30] F. D. Becchetti, Jr. and G. W. Greenlees, Nucleon-nucleus optical-model parameters, $A > 40$, $E < 50$ MeV, Phys. Rev. **182**, 1190 (1969).
[31] R. L. Varner, W. J. Thompson, T. L. McAbee, E. J. Ludwig, and T. B. Clegg, A global nucleon optical model potential, Phys. Rep. **201**, 57 (1991).
[32] W. W. Daehnick, J. D. Childs, and Z. Vrcelj, Global optical model potential for elastic deuteron scattering from 12 to 90 MeV, Phys. Rev. C **21**, 2253 (1980).
[33] C. E. Busch, T. B. Clegg, S. K. Datta, and E. J. Ludwig, The cross section and vector analyzing power for the elastic scattering of 15.0 MeV deuterons from ^{10}B, ^{12}C, ^{13}C, ^{14}N, and ^{16}O, Nucl. Phys. A **223**, 183 (1974).
[34] I. J. Thompson, Coupled reaction channels calculations in nuclear physics, Comput. Phys. Rep. **7**, 167 (1988); http://www.fresco.org.uk
[35] M. H. Macfarlane and S. C. Pieper, *PTOLEMY, A Program for Heavy-ion Direct-reaction Calculations*, ANL-76-11 Rev.1, Argonne National Lab, 1976.
[36] H. Fuchs, K. Grabisch, P. Kraaz, and G. Röschert, States in ^{12}C and ^{16}O investigated by the ^{11}B(d,n) and ^{15}N(d,n) reactions, Nucl. Phys. A **105**, 590 (1967).
[37] G. S. Mutchler, D. Rendic, D. E. Velkley, W. E. Sweeney, Jr., and G. C. Phillips, The (d,n) reaction on 1p shell nuclei at $E_d = 11.8$ MeV, Nucl. Phys. A **172**, 469 (1971).
[38] J. Bommer, H. Fuchs, K. Grabisch, U. Janetzki, and G. Röschert, Study of ^{15}O states by the ^{14}N(d,n) reaction, Nucl. Phys. A **172**, 618 (1971).
[39] W. Bohne, J. Bommer, H. Fuchs, K. Grabisch, H. Kluge, and G. Röschert, Study of the (d,n) and (d,p) reactions on ^{15}N, Nucl. Phys. A **196**, 41 (1972).
[40] A. W. Barrows, Jr., F. Gabbard, and J. L. Weil, ^{19}F$(d,n)^{20}$Ne Reaction from 2.5 to 6.5 MeV, Phys. Rev. **161**, 928 (1967).
[41] P. Bem *et al.*, Asymptotic normalization coefficients for ^{14}N-^{13}C + p from ^{13}C$(^3$He$,d)^{14}$N, Phys. Rev. C **62**, 024320 (2000).
[42] S. Cohen and D. Kurath, Spectroscopic factors for the 1p shell. Nucl. Phys. A **101**, 1 (1967).
[43] S. Varma and P. Goldhammer, Wave functions in 1p shell nuclei, Nucl. Phys. A **125**, 193 (1969).
[44] V. R. Pandharipande, I. Sick, and P. K. A. de Witt Huberts, Independent particle motion and correlations in fermion systems. Rev. Mod. Phys. **69**, 981 (1997).
[45] N. K. Timofeyuk, New Insight Into Observation of Spectroscopic Strength Reduction in Atomic Nuclei: Implication for the Physical Meaning of Spectroscopic Factors, Phys. Rev. Lett. **103**, 242501 (2009).
[46] W. Liu *et al.*, Measurement of the Angular distribution for the ^{7}Be$(d,n)^8$B reaction and determination of the astrophysical S factor for the ^{7}Be$(p,\gamma)^8$B reaction, Nucl. Instrum. Methods Phys. Res. A **616**, 131 (1997).
[47] F. D. Becchetti, R. S. Raymond, R. O. Torres-Isea, A. Di Fulvio, S. D. Clarke, S. A. Pozzi, and M. F. Febbraro, Recent developments in deuterated scintillators for neutron measurements at low-energy accelerators, CAARI 2016 Conference (to be published).
[48] A. Di Fulvio, F. D. Becchetti, R. S. Raymond, R. O. Torres-Isea, S. D. Clarke, and S. A. Pozzi, Characterization of deuterated-xylene scintillator as a neutron spectrometer, IEEE Trans. Nucl. Sci. **64**, 1825 (2017).
[49] M. Febbraro, The ^{13}C$(\alpha,n)^{16}$O reaction: A background source for underground astrophysics measurements and neutrino measurements, 2016 CAARI Conference Abstracts, October 2016.